Consistent numerical evaluation of the anchoring energy of a grooved surface

Jun-ichi Fukuda (福田順一),[1,2,*] Makoto Yoneya (米谷慎),[1,2] and Hiroshi Yokoyama (横山浩)[1,2]
[1]*Nanotechnology Research Institute, National Institute of Advanced Industrial Science and Technology (AIST), 1-1-1 Umezono, Tsukuba 305-8568, Japan*
[2]*Liquid Crystal Nano-System Project, ERATO/SORST, Japan Science and Technology Agency, 5-9-9 Tokodai, Tsukuba 300-2635, Japan*
(Received 10 October 2008; published 16 January 2009)

We evaluate the azimuthal anchoring energy of a grooved surface by calculating numerically the Frank elastic energy of a nematic cell composed of the grooved surface and a flat one with rigid azimuthal anchoring, where the director is fixed along the ϕ direction. We pay attention to the surface anchoring induced by elastic distortions of the director due to its contact with a nonflat surface, which impose local planar degenerate anchoring. Surface anchoring of this kind was analyzed analytically for shallow grooves by Berreman [Phys. Rev. Lett. **28**, 1683 (1972)] and critically reexamined by the present authors [Phys. Rev. Lett. **98**, 187803; **99**, 139902(E) (2007)]. We consider two types of surface. one is a surface with one-dimensional sinusoidal parallel grooves, and the other is a surface with two-dimensional square patterns whose surface height is given by a sum of two sinusoidal functions with orthogonal wave vectors. The total energy is the sum of the anchoring energy and the twist energy in the bulk. For the calculation of the twist energy to be eliminated and the evaluation of the azimuthal-angle dependence of the anchoring energy, the "average" azimuthal angle at the bottom, $\varphi(0)$, must be determined. We adopt two methods to determine $\varphi(0)$. One is a simple extrapolation of the twist deformation in the bulk. The other relates $\varphi(0)$ to the variation of the total Frank elastic energy with respect to ϕ. Our calculations indicate that both methods give essentially the same results, which indicates the consistency of those two methods. We also show that, for a surface with square patterns, the agreement between theory and numerical calculations is quite good even when the maximum of the surface slope is around 0.4, which theory assumes is much smaller than unity. When the surface slope is of order unity, the deviation of numerical results from theory crucially depends on the the surface elastic constant K_{24}.

DOI: 10.1103/PhysRevE.79.011705 PACS number(s): 61.30.Hn, 61.30.Dk

I. INTRODUCTION

Control of the properties of surface anchoring in a desirable manner is crucial in applications involving liquid crystals, such as display technologies. Understanding the underlying mechanism of surface anchoring is an important subject also in the fundamental science of liquid crystals [1–3].

Two mechanisms have been shown to be mainly responsible for surface anchoring. One is intermolecular interaction between the liquid crystal molecules and the ones constituting the surface [4–6], which are polymer chains in most practical cases. This mechanism of surface anchoring, although important, is difficult to deal with physically because of its sensitivity to chemical details of the constituent molecules. The other mechanism is elastic distortions of the liquid crystals arising from their contact with a nonflat surface. The latter has been attracting considerable attention because recent rapid progress in nanotechnology has enabled one to tailor arbitrarily patterned or grooved surfaces with submicrometer-scale precision, leading to many experimental studies aimed at achieving some desirable anchoring properties on microscopically grooved surfaces [7–15]. Anchoring properties realized by such surfaces include multistability [9,14] and controllable pretilt angles [10,11,15].

The first theoretical study concerning surface anchoring attributable to nonflat surface geometry and the resultant elastic distortion of a nematic liquid crystal was presented by Berreman [16]. His theory has been regarded as capturing the essential aspects of surface anchoring induced by surface geometry, and motivated numerous theoretical [17–21] as well as experimental studies [22–24] to elucidate the effect of surface geometry on liquid crystal anchoring. In our recent work, however, we showed that Berreman's theory was based on the invalid assumption of no azimuthal director distortions and did not incorporate surface elasticity properly. We presented a rigorous analytic formula for the azimuthal anchoring energy of a nematic liquid crystal for surfaces with one-dimensional parallel grooves [25,26] and extended our theory to surfaces with arbitrary patterns [27].

However, all of the analytical studies, including ours, concerning anchoring induced by nonflat surface geometry rely on the assumption that the surface slope and the resultant distortion of a nematic liquid crystal are small enough so that it is sufficient to consider the quadratic form of the Frank elastic energy in terms of the director distortion. Otherwise, the Euler-Lagrange equations to minimize the Frank elastic energy become nonlinear in the director $\boldsymbol{n}$, which are, in practically all cases we are interested in, impossible to solve analytically. Therefore numerical studies will be necessary for understanding the anchoring properties of grooved surfaces with relatively large slope. There have been a number of numerical studies based on continuum theory [28–32] or molecular dynamics simulations [33] to elucidate the behavior of a nematic liquid crystal in the vicinity of a grooved surface. However, none of those previous studies has paid attention to the precise form of the anchoring energy as a

*fukuda.jun-ichi@aist.go.jp

function of the azimuthal angle of the director.

In our previous study [34], we carried out a numerical analysis of the anchoring energy of a surface with one-dimensional parallel grooves to check the validity of our analytic studies [25,26] and to find out to what extent our theory is applicable (or to be precise, up to how large a surface slope our theory is valid). We showed that for $qA \lesssim 0.2$, with q and A being the wave number and the amplitude of the sinusoidal profile of the grooves, respectively, our numerical results of the azimuthal-angle dependence of the anchoring energy agree perfectly with analytical ones. Even when qA is of order unity, the deviations of numerical results from analytical ones are relatively small, indicating the unexpectedly wide applicability of our analytical theory.

Since our previous paper [34] was a short contribution, in the present paper we will present some more details of our numerical calculations, including how to discretize the Frank elastic energy. We will also discuss in more detail how the anchoring energy should be evaluated from the calculated Frank elastic energy; contributions from the twist in the bulk must be carefully eliminated and the evaluation of the azimuthal angle of the director at the grooved surface is nontrivial. Furthermore, we will present our results of the calculation of the anchoring energy of surfaces with two-dimensional square patterns, while our previous work [34] was restricted to a discussion on one-dimensional parallel grooves.

This paper is organized as follows. In Sec. II, we briefly review the results of our previous studies [25–27] which should be compared to our numerical results. Section III describes the details of our numerical calculations. We will present our results in Sec. IV. Section V concludes this paper.

II. THEORY

Let us now review briefly our analytical theory [25–27] on surface anchoring due to surface grooves, which originates from a critical reexamination of the well-known Berreman theory on the same problem [16]. We first discuss the anchoring induced by one-dimensional sinusoidal grooves parallel to the x axis, whose surface height $h(x,y)$ with respect to a reference plane $z=0$ is written as

$$h(x,y) = A \sin qy \tag{1}$$

with $q>0$. We consider a situation in which a nematic liquid crystal is in contact with the surface described above, and the orientation at infinity $z=+\infty$ is along $\boldsymbol{n}_\infty=(\cos\phi,\sin\phi,0)$. The azimuthal angle ϕ is then the one between $\boldsymbol{n}_\infty$ and the groove direction.

The Frank elastic energy of a nematic liquid crystal in terms of the director $\boldsymbol{n}$ is written as [1,35,36]

$$f_{\mathrm{Frank}}\{\boldsymbol{n},\nabla\boldsymbol{n}\} = \frac{1}{2}[K_1(\nabla\cdot\boldsymbol{n})^2 + K_2(\boldsymbol{n}\cdot\nabla\times\boldsymbol{n})^2 + K_3(\boldsymbol{n}\times\nabla\times\boldsymbol{n})^2 - K_s\nabla\cdot(\boldsymbol{n}\nabla\cdot\boldsymbol{n}+\boldsymbol{n}\times\nabla\times\boldsymbol{n})]. \tag{2}$$

Here K_1, K_2, and K_3 are the splay, twist, and bend elastic constants, respectively. The last term, which can be converted to a surface integral, is referred to as the surface elastic term. For the clarification of the role of the surface elastic term, we have introduced a symbol $K_s \equiv K_2 + K_{24}$, where K_{24} is the saddle-splay elastic constant [35–37]. Here we do not consider another surfacelike term $K_{13}\nabla\cdot(\boldsymbol{n}\nabla\cdot\boldsymbol{n})$, because this term renders the problem of finding the director profile minimizing the Frank elastic energy ill defined [35,38], and even the presence of this term (or nonzero K_{13}) has been questioned [39].

We assume local planar degenerate anchoring at the surface: That is, the director $\boldsymbol{n}$ can point along any direction without any energetic cost as long as it is tangential to the surface. When $\phi\neq 0$, this planar alignment induces elastic distortions of the director $\boldsymbol{n}$. Under the assumption of small surface slope, i.e., $|qA|\ll 1$, the problem of finding the equilibrium director profile minimizing the total Frank elastic energy is analytically tractable. From the calculated director profile, we can determine the anchoring energy due to the elastic distortion arising from surface grooves. The details of the calculations are given in our previous work [25,26], and the final result of the anchoring energy per unit surface reads

$$f_{1\mathrm{D}}(\phi) = \frac{1}{4}A^2q^3\frac{\sin^2\phi}{g_1(\phi)}\left[K_3\sin^2\phi + K_s\cos^2\phi \times\left(2 - \frac{K_s}{K_3}\frac{g_1(\phi)g_2(\phi)-\cos^2\phi}{\sin^2\phi}\right)\right], \tag{3}$$

where $g_i(\phi)=\sqrt{\cos^2\phi+(K_3/K_i)\sin^2\phi}$ $(i=1,2)$.

The above theory on one-dimensional sinusoidal grooves can be readily extended to surfaces of arbitrary shape, as long as the surface slope is small enough [27]. A simple superposition principle applies; when we write the surface height profile $h(x,y)$ in terms of a Fourier series, the resultant anchoring energy is just the sum of the contributions from each Fourier component. In the simple case of a surface with square patterns whose height is

$$h(x,y) = A(\sin qx + \sin qy), \tag{4}$$

the anchoring energy $f_{\mathrm{sq}}(\phi)$ is simply written using the above result, Eq. (3), as

$$f_{\mathrm{sq}}(\phi) = f_{1\mathrm{D}}(\phi) + f_{1\mathrm{D}}(\phi+\pi/2). \tag{5}$$

III. NUMERICAL CALCULATION

A. Calculation of the equilibrium profile

What we calculate numerically is essentially the same as in our theory: calculation of the Frank elastic energy of a nematic liquid crystal in contact with a grooved surface imposing local planar degenerate anchoring. One difference is that in our numerical calculations we adopt the complete form of the Frank energy, Eq. (2). On the other hand, in analytical arguments with the assumption of small distortion of $\boldsymbol{n}$, only a quadratic form in the distortion has been used [16,25–27]. Moreover, while in our theory we have dealt with a semi-infinite space $h(x,y)\leqslant z\leqslant+\infty$, in our numerical calculations we consider a finite cell in which a liquid crystal

is filled in the region $h(x,y) \leqslant z \leqslant L_z < +\infty$, with L_z being the position of the upper flat surface. This is because in general special care is necessary in numerical calculations when one wants to treat infinity. The difference arising from the choice of a finite system will be given in detail later.

As in the previous section, we consider two types of grooved surface. One is a set of parallel grooves whose height is $h(x,y)=A \sin qy$; the other is a surface with square patterns: $h(x,y)=A(\sin qx+\sin qy)$. Hereafter we describe our numerical treatment in the case of a surface with square patterns. In the case of a set of parallel grooves, due to translational symmetry along the x direction, $\partial_x=0$, and we have to deal only with a two-dimensional rectangular system in the (y,ζ) space (the definition of ζ is given below). The details of the treatment of this two-dimensional system can be found in our previous paper [34].

We adopt periodic boundary conditions in the x and y directions that conform to the periodicity of the surface; the director profile satisfies $\boldsymbol{n}(x,y,z)=\boldsymbol{n}(x+2\pi k/q, y+2\pi l/q, z)$, with k and l being arbitrary integers. We also introduce a variable $\zeta(x,y,z)$ satisfying

$$z = \zeta + (1 - \zeta/L_z)h(x,y). \tag{6}$$

Then our system in the (x,y,z) space with $0 \leqslant x,y < L_x = L_y = 2\pi/q$ and $h(x,y) \leqslant z \leqslant L_z$ is mapped onto a rectangular solid in the (x,y,ζ) space with $0 \leqslant \zeta \leqslant L_z$.

The total Frank elastic energy per unit area of the reference plane $(z=0)$ is given by

$$F = \left(\frac{q}{2\pi}\right)^2 \int_0^{2\pi/q} dx \int_0^{2\pi/q} dy \int_0^{L_z} d\zeta \frac{\partial z}{\partial \zeta} \times f_{\mathrm{Frank}}\{\boldsymbol{n}, \partial_x \boldsymbol{n}(x,y,\zeta), \partial_y \boldsymbol{n}(x,y,\zeta), \partial_\zeta \boldsymbol{n}(x,y,\zeta)\}. \tag{7}$$

We discretize our system in a three-dimensional (x,y,ζ) space by $N \times N \times (N+1)$ grid points with equal spacings, $\Delta x = \Delta y = L_{x,y}/N = 2\pi/qN$ and $\Delta\zeta = L_z/N$. In the present calculation, we choose $N=32$ and $L_z = L_{x,y}$. At each grid point, we assign the values of the director as $\boldsymbol{n}_{i,j,k} = \boldsymbol{n}(x=i\Delta x, y=j\Delta y, \zeta=k\Delta\zeta)$, with $0 \leqslant i, j < N$ and $0 \leqslant k \leqslant N$. How to discretize Eq. (7) and calculate functional derivatives $\delta F/\delta \boldsymbol{n}$ in a numerical sense will be given in Appendix A.

We obtain the equilibrium director profile by relaxing the system via a simple equation involving the rotation of the director: $\partial n_i/\partial t = (\delta_{ij} - n_i n_j)\delta F/\delta n_j$ [40], where a hydrodynamic flow is not taken into account. In the present study, we are interested only in the equilibrium profiles of $\boldsymbol{n}$, and therefore there is no problem neglecting the effect of hydrodynamics. The time t is rescaled so that rotational viscosity does not appear explicitly in the above dynamical equation. To take care of the constraint of $|\boldsymbol{n}|=1$, we employ the explicit Euler scheme $[\tilde{n}_i(t+\Delta t) - n_i(t)]/\Delta t = [\delta_{ij} - n_i(t)n_j(t)]\delta F/\delta n_j(t)$ and set $\boldsymbol{n}(t+\Delta t) = \tilde{\boldsymbol{n}}(t+\Delta t)/|\tilde{\boldsymbol{n}}(t+\Delta t)|$.

In the course of the relaxation we fix the director at the upper surface $z=\zeta=L_z$ to $\boldsymbol{n}_{i,j,N}=(\cos\phi, \sin\phi, 0)$. At the lower surface $\zeta=0$, the tangential boundary condition is imposed; i.e., $\boldsymbol{n}_{i,j,0} \cdot \boldsymbol{\nu}_{i,j} = 0$, with $\boldsymbol{\nu}_{i,j} = \boldsymbol{0}$ being the surface normal at $x=i\Delta x$ and $y=j\Delta y$.

As the initial condition for the relaxation, we employ uniform alignment $\boldsymbol{n}_{i,j,k}=(\cos\phi, \sin\phi, 0)$ when $0 < \phi \leqslant \pi/4$. In some cases with large qA, we also perform calculations with $\phi \leqslant 0$ [see Fig. 12(b) below]. In such cases, an equilibrium profile for $\phi = 2.5°$ is used as the initial condition.

B. Determination of the azimuthal-angle dependence of the anchoring energy

From the calculation of the equilibrium profile of $\boldsymbol{n}$ and the resultant Frank elastic energy (7) with the variation of the azimuthal angle ϕ at the upper surface, we can deduce the azimuthal-angle dependence of the anchoring energy. However, care must be taken in interpreting the calculation results, because we are dealing with a finite cell and twist deformation is present in the bulk. Therefore, we must eliminate the contribution from the twist deformation in the bulk.

To discuss the effect of twist deformation in the bulk, we consider a simplified model of a nematic cell with thickness L_z sandwiched by two parallel flat surfaces. As in our numerical system, the director at the upper surface $(z=L_z)$ is fixed to $\boldsymbol{n}=(\cos\phi, \sin\phi, 0)$. The lower surface $(z=0)$ assumes planar alignment whose anchoring energy per unit area is $\tilde{f}_{\mathrm{a}}(\varphi(0))$, where $\varphi(0)$ is the azimuthal angle of the director at the lower surface and now $\tilde{f}_{\mathrm{a}}(\varphi(0))$ is an unknown function of $\varphi(0)$. The director $\boldsymbol{n}$ in the bulk is a function of only z and is written as $\boldsymbol{n}(z)=(\cos\varphi(z), \sin\varphi(z), 0)$, with $\varphi(L_z)=\phi$. The twist energy is minimized when $d\varphi/dz = \mathrm{const} = [\phi - \varphi(0)]/L_z$. Then the total free energy of the cell per unit area is written as

$$F(\phi) = \tilde{f}_{\mathrm{a}}(\varphi(0)) + \frac{K_2}{2}\int_0^{L_z} dz \left(\frac{d\varphi}{dz}\right)^2 = \tilde{f}_{\mathrm{a}}(\varphi(0)) + \frac{K_2(\phi - \varphi(0))^2}{2L_z}. \tag{8}$$

Recall that both $\tilde{f}_{\mathrm{a}}$ and $\varphi(0)$ are unknown at present. However, since $F(\phi)$ has been calculated numerically, once the relation between $\varphi(0)$ and ϕ is known, the anchoring energy $\tilde{f}_{\mathrm{a}}$ can be obtained as a function of $\varphi(0)$. In what follows we describe two ways of determining the relation between $\varphi(0)$ and ϕ.

One is the method used in our previous study [34]: extrapolation of the uniform twist in the bulk. To be precise, we first calculate the azimuth $\varphi_{\boldsymbol{n}}$ of the director $\boldsymbol{n}$, that is, $\varphi_{\boldsymbol{n}} \equiv \arctan(n_y/n_x)$, at all the grid points in $z \geqslant L_z/2$. Then we determine $\varphi(0)$ by a least squares fit of those $\varphi_{\boldsymbol{n}}$'s to $\varphi(z) = \varphi(0) + [\phi - \varphi(0)]z/L_z$. We will refer to this evaluation of $\varphi(0)$ as method A.

The other is the use of Eq. (8). Recall that, for our simplified cell to be in equilibrium, $F(\phi)$ in Eq. (8) must be minimized with respect to $\varphi(0)$. Therefore

$$0 = \tilde{f}_{\mathrm{a}}'(\varphi(0)) - \frac{K_2[\phi - \varphi(0)]}{L_z} \tag{9}$$

is satisfied, in which $\tilde{f}_{\mathrm{a}}'(\varphi) = d\tilde{f}_{\mathrm{a}}(\varphi)/d\varphi$. Equation (9) just describes the balance of torque at the lower surface.

We note that under the constraint of Eq. (9) $\varphi(0)$ varies with the variation of ϕ. Thus the differentiation of Eq. (8) with respect to ϕ yields

$$\frac{dF(\phi)}{d\phi} = \tilde{f}_a'(\varphi(0))\frac{d[\varphi(0)]}{d\phi} + \frac{K_2[\phi - \varphi(0)]}{L_z}\left(1 - \frac{d[\varphi(0)]}{d\phi}\right)$$
$$= \frac{K_2[\phi - \varphi(0)]}{L_z}, \tag{10}$$

where use has been made of Eq. (9) to eliminate $\tilde{f}_a'(\varphi(0))$. Equation (10) indicates that the relation between $\varphi(0)$ and ϕ can be deduced when the variation of the total Frank elastic energy F with respect to ϕ is known. We will refer to this treatment as method B. It is instructive to note that the left-hand side of Eq. (10) is the work necessary to rotate the upper plane (imposing rigid azimuthal anchoring) by unit angle. Therefore the azimuthal angle $\varphi(0)$ at the lower plane is known directly by measuring the work required to rotate the upper plane.

Now we comment on the advantages and disadvantages of methods A and B. While method A can be readily implemented and its implication can be easily understood, the evaluation of the uniform twist from the calculated data might need a careful treatment. Method B is based on the properties of the (model) system derived rigorously [Eq. (10)], and is therefore expected to be more accurate than method A. However, method B needs a numerical evaluation of $dF(\phi)/d\phi$, and therefore many numerical data with small intervals of ϕ will be necessary.

From the treatments described above, we can determine the azimuthal-angle $[\varphi(0)]$ dependence of the surface anchoring energy $\tilde{f}_a$ by calculating numerically the ϕ dependence of the total Frank elastic energy F. In the following section, we will present our numerical results of the evaluation of the anchoring energies.

IV. RESULTS AND DISCUSSIONS

In our numerical calculations, we have chosen the material parameters $K_1/K_3=0.7$, $K_2/K_3=0.5$, and $K_s/K_3=0.6$ or 1 as in our previous study [34]. Notice the inequality $K_3>K_1>K_2$ satisfied by most rodlike liquid crystals, which conforms to our choice of K_1/K_3 and K_2/K_3.

Now we comment on the inequalities that must be satisfied by the surface elastic constant. Ericksen showed [36,41] that for the Frank elastic energy (2) to be positive definite, a set of inequalities must be satisfied. In our choice with $K_1>K_2>0$ and $K_3>0$, one of the inequalities reads

$$|K_{24}| \leqslant K_2 \quad \text{or} \quad 0 \leqslant K_s \leqslant 2K_2. \tag{11}$$

Notice also that, from their molecular theory, Nehring and Saupe [37] derived an equality $2K_{24}=K_1-K_2$, or $2K_s=K_1+K_2$. After a careful reexamination of their molecular theory, Yokoyama [39] replaced the equality by an inequality

$$2K_{24} \geqslant K_1 - K_2 \quad \text{or} \quad 2K_s \geqslant K_1 + K_2. \tag{12}$$

Therefore $K_s/K_3=0.6$ and 1 are the smallest and the largest values allowed by the inequalities (11) and (12).

A. One-dimensional parallel grooves

In our previous study [34], we presented our numerical evaluation of the anchoring energy of one-dimensional parallel grooves using method A described above. Thus we now concentrate on the difference arising from the choice of method A or B. The height profile of the surface is given in Eq. (1).

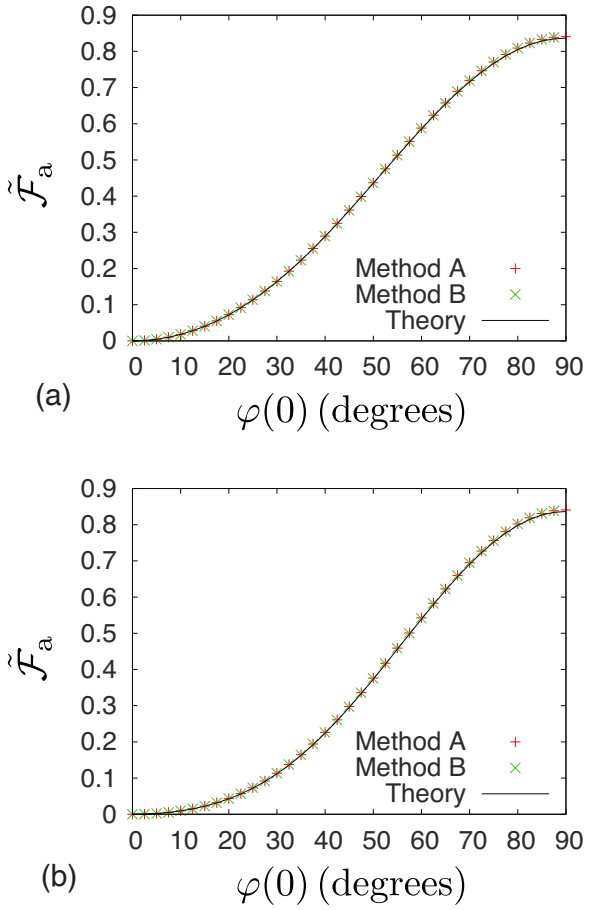

FIG. 1. (Color online) Rescaled anchoring energy $\tilde{\mathcal{F}}_a$ for one-dimensional parallel grooves as a function of the azimuthal angle at the bottom, $\varphi(0)$ for $qA=\pi/160\simeq 0.0196$. The surface elastic constant is $K_s/K_3=0.6$ (a) and 1 (b). The solid lines represent the rescaled analytic anchoring energy $\mathcal{F}_a$ for small qA.

In Figs. 1–3, we plot the azimuthal angle $[\varphi(0)]$ dependence of the calculated anchoring energy evaluated by methods A and B for $qA=\pi/160\simeq 0.0196$, $\pi/16\simeq 0.196$, and $3\pi/16\simeq 0.589$, respectively. Here we have introduced a rescaled numerical anchoring energy $\tilde{\mathcal{F}}_a(\varphi(0)) \equiv \tilde{f}_a(\varphi(0))/(\frac{1}{4}K_3A^2q^3)$. We also show there a rescaled analytical anchoring energy $\mathcal{F}_a=f_{1D}/(\frac{1}{4}K_3A^2q^3)$, in which the definition of f_{1D} is found in Eq. (3). It can be seen from Figs. 1–3 that methods A and B yield almost the same dependence of the anchoring energy on the azimuthal angle $\varphi(0)$. Moreover, as has already been shown in our previous work [34], for $qA=\pi/160$ and $\pi/16$, the anchoring energies calculated numerically show excellent agreement with analytical ones. These results clearly guarantee the validity of our numerical evaluation of the anchoring energy, by both methods A and B.

To see the difference in methods A and B in another way, we plot in Figs. 4–6, the dependence of the calculated azimuthal angle $\varphi(0)$ at the grooved surface on the (fixed) azi-

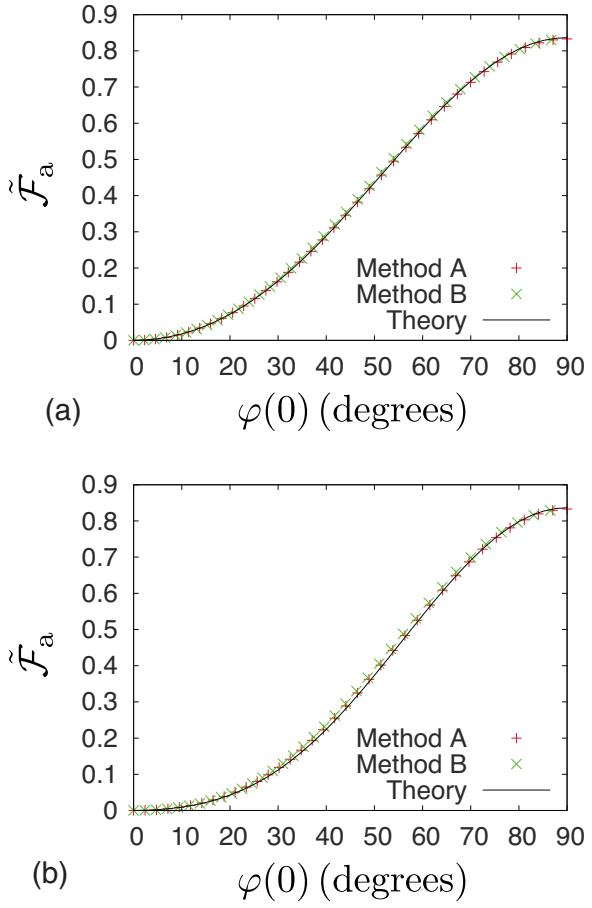

FIG. 2. (Color online) Same as Fig. 1 for $qA=\pi/16\simeq 0.196$.

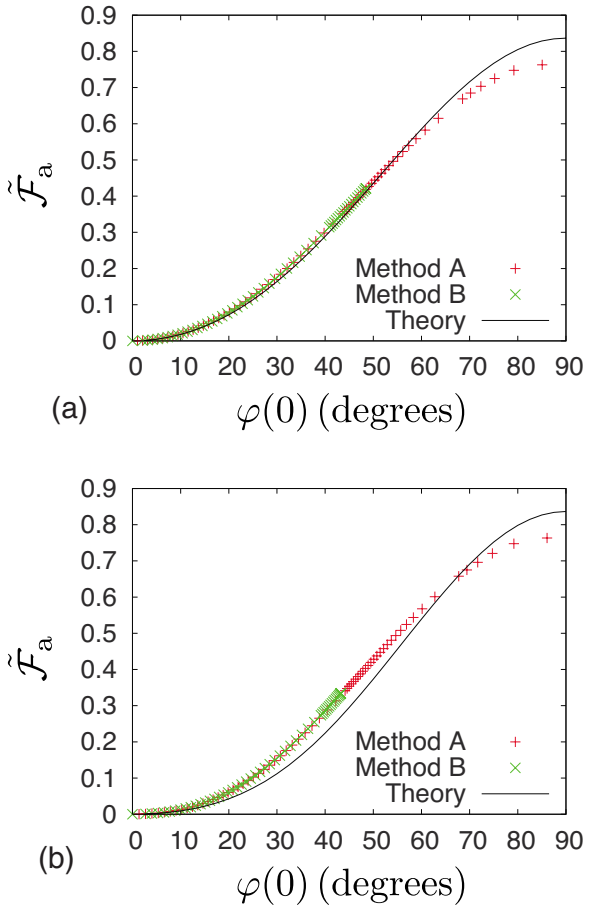

FIG. 3. (Color online) Same as Fig. 1 for $qA=3\pi/16\simeq 0.589$.

muthal angle ϕ at the top flat surface. For $qA=\pi/160$ (Fig. 4), the calculated $\varphi(0)$'s fall on to the line $\varphi(0)=\phi$, indicating that there is no observable twist in the bulk. For $qA=\pi/16$ in Fig. 5, a slight deviation from $\varphi(0)=\phi$ is observed, and except when $\phi=0°$ or 90°, $\varphi(0)<\phi$, which implies that the director at the bottom grooved surface is rotated towards the easy direction $\varphi(0)=0°$ and thus twist deformation is present in the bulk. The results from methods A and B differ slightly; nevertheless the behaviors of the anchoring energy deduced from methods A and B are almost the same, as has already been seen in Fig. 2. This somewhat surprising result again manifests the validity of both methods A and B for the calculation of the anchoring energy. We also speculate that the difference in the behavior of $\varphi(0)$ with respect to ϕ obtained by methods A and B arises from the finite size effect; when the system thickness L_z goes to infinity, it is expected that the difference will vanish.

In contrast to the previous cases, large deviation from $\varphi(0)=\phi$ is clearly seen in Fig. 6 when $qA=3\pi/16$. As has already been noted in our previous work [34], $\varphi(0)\neq 90°$ even when $\phi=90°$. These results clearly imply that large twist deformations exist in the bulk. We also find from Fig. 6 that methods A and B give almost, but not perfectly, the same results for $\varphi(0)$ unless $\phi\gtrsim 90°$. Here again it is surprising that the results of the calculation of the anchoring energy using methods A and B fall onto the same curve, as indicated in Fig. 3.

It is seen from Fig. 6 that for $qA=3\pi/16$, $\varphi(0)$ determined by method B does not exceed some value $\varphi(0)_{\max}$ smaller than 90°, which marks a sharp contrast to the behavior of $\varphi(0)$ for $qA=\pi/160$ and $\pi/16$, as found in Figs. 4 and 5. This finding for $qA=3\pi/16$, together with the fact that $\varphi(0)\neq 90°$ even when $\phi=90°$ as mentioned above, can be explained in a simple schematic manner presented in Appendix B.

B. Two-dimensional square patterns

Now let us move on to the cases of a surface with square patterns whose surface height is written as Eq. (4). Figures 7–9 show the azimuthal angle ($\varphi(0)$) dependence of the calculated anchoring energy evaluated by methods A and B for $qA=\pi/160\simeq 0.0196$, $\pi/16\simeq 0.196$, and $3\pi/16\simeq 0.589$, respectively. The rescaled numerical anchoring energy is defined as $\tilde{\mathcal{F}}_a(\varphi(0))\equiv[\tilde{f}_a(\varphi(0))-\tilde{f}_a(45°)]/(\frac{1}{4}K_3A^2q^3)$ and the same definition is employed for the rescaled analytical anchoring energy $\mathcal{F}_a(\varphi(0))$. The form of the unrescaled analytical anchoring energy is found in Eq. (5). Note that, from the symmetry of square patterns, it is sufficient to show the results for $0°\leqslant\varphi(0)\leqslant 45°$.

As in the cases of one-dimensional grooves in the previous section, we find from Figs. 7–9 that methods A and B result in almost the same dependence of the anchoring en-

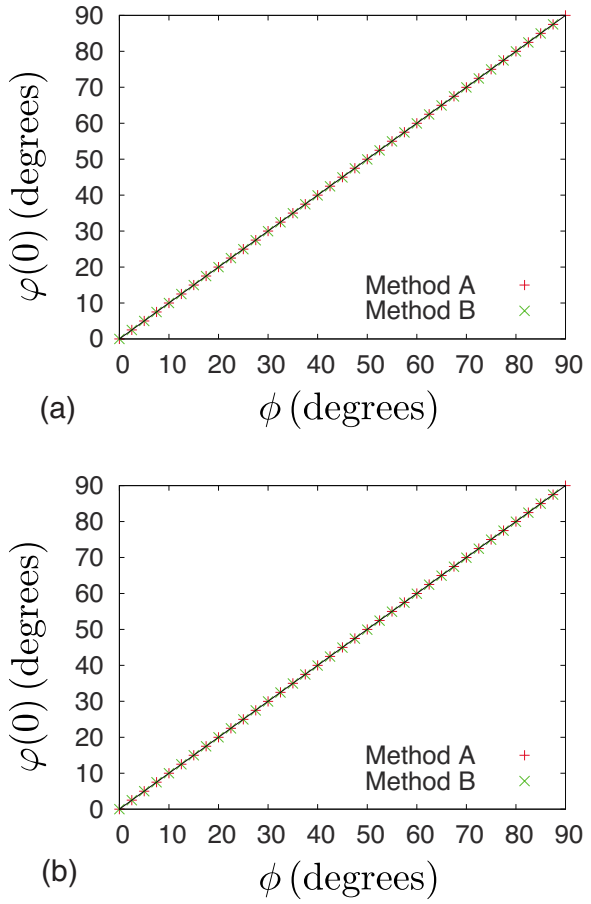

FIG. 4. (Color online) Azimuthal angle of the director at the bottom one-dimensionally grooved surface, $\varphi(0)$, as a function of the (fixed) azimuthal angle at the top flat surface ϕ for $qA=\pi/160\simeq 0.0196$. The surface elastic constant is $K_s/K_3=0.6$ (a) and 1 (b). The solid line corresponds to $\varphi(0)=\phi$, which implies the absence of twist deformations in the bulk.

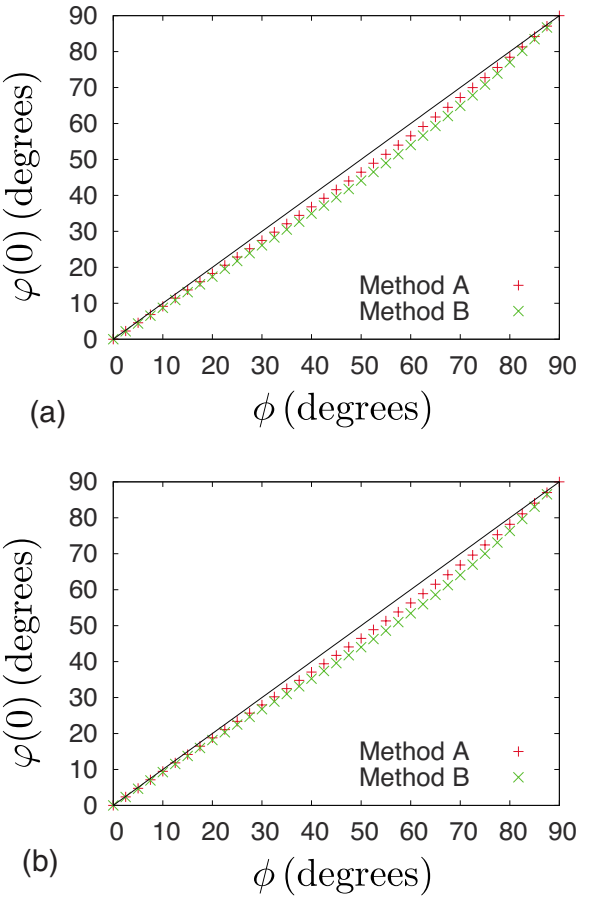

FIG. 5. (Color online) Same as Fig. 4 for $qA=\pi/16\simeq 0.196$.

ergy on $\varphi(0)$, again indicating the validity of both methods A and B as the way of evaluating the anchoring energy numerically. It can be also seen from Figs. 7 and 8 that for $qA=\pi/160$ and $\pi/16$, the numerical anchoring energies agree quite well with analytical ones. Notice from Eq. (4) that the maximum slope of the surface pattern is $2qA$ and for $qA=\pi/16$ (Fig. 8), $2qA\simeq 0.393$, which cannot be regarded as much smaller than unity. Since the assumption $|qA|\ll 1$ is employed in the theory as already noted, the agreement with theory and numerical calculation even when the maximum slope is around 0.4 is again quite surprising.

In the case of $qA=3\pi/16$, where the maximum slope is 1.18, deviations of numerical results from theory is visible. However, an important qualitative feature in the analytical result that the minimum of the anchoring energy is located at $\varphi(0)=45°$ is retained in our numerical results. We also find that the relative difference between theory and numerical results is larger for $K_s/K_3=1$ than for $K_s/K_3=0.6$, which indicates the crucial role of surface elasticity in surface anchoring. We will return to this problem later why $K_s/K_3=0.6$ gives a relatively better agreement.

We also comment that $\tilde{\mathcal{F}}_a(0°)$ (or the difference between the rescaled anchoring energies at $\varphi(0)=0°$ and 45°) is larger for $K_s/K_3=1$ than for $K_s/K_3=0.6$ (look carefully at the vertical axes in Figs. 7–9). This result again demonstrates the importance of surface elasticity and shows a marked difference from the cases one-dimensional grooves, where $\tilde{\mathcal{F}}_a(90°)$ [or the difference between the anchoring energies at $\varphi(0)=0°$ and 90°] does not depend on K_s.

As in the previous section, to check the difference in methods A and B in another way, we present in Figs. 10–12, the dependence of the calculated azimuthal angle $\varphi(0)$ at the grooved surface on the fixed azimuthal angle ϕ at the top flat surface. Figure 10 for $qA=\pi/160$ clearly shows that $\varphi(0)$ falls on the line $\varphi(0)=\phi$, indicating the absence of twist in the bulk as in the case of one-dimensional grooves in Fig. 4. For $qA=\pi/16$ in Fig. 11, we can observe a slight deviation from $\varphi(0)=\phi$. It is also seen that $\varphi(0)$ is always larger than ϕ except at $\phi=0°$ and 45°, which means the rotation of the director at the bottom surface toward the easy direction $\varphi(0)=45°$. This tendency is similar to that in Fig. 5 for one-dimensional grooves, except for the difference in the direction of the easy axis [in the latter case it is along $\varphi(0)=0°$]. We find, as in Fig. 5, that the results from methods A and B differ slightly. However, despite this difference, the anchoring energies calculated from methods A and B fall on a single curve, again indicating the robustness of the calculation methods for the anchoring energy.

Figure 12 plots $\varphi(0)$ for $qA=3\pi/16$. Both for K_s/K_3 =(a) 0.6 and (b) 1, large twist deformations are clearly ob-

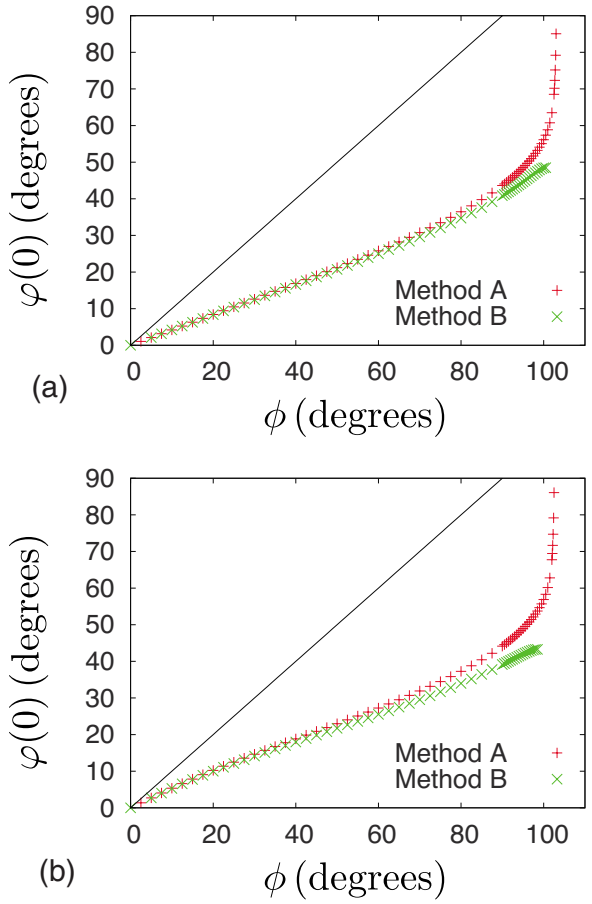

FIG. 6. (Color online) Same as Fig. 4 for $qA=3\pi/16\simeq 0.589$.

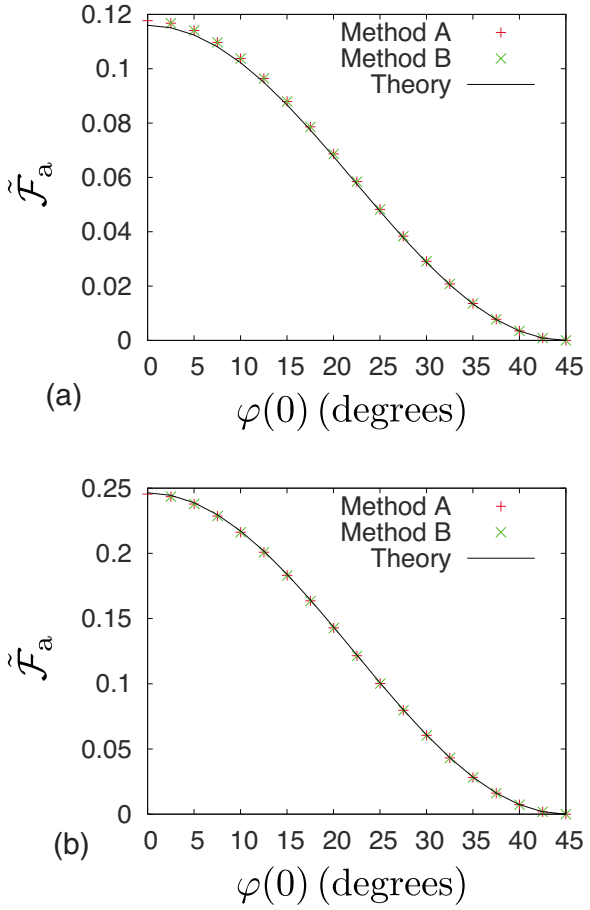

FIG. 7. (Color online) Plots of the rescaled anchoring energy $\tilde{\mathcal{F}}_a$ for a surface with square pattern as a function of the azimuthal angle at the bottom, $\varphi(0)$ for $qA=\pi/160\simeq 0.0196$. The surface elastic constant is $K_s/K_3=0.6$ for (a) and $K_s/K_3=1$ for (b). The solid lines represent the rescaled analytic anchoring energy $\mathcal{F}_a$ for small qA.

served. However a difference is found there; in Fig. 12(a), $\varphi(0)=0°$ at $\phi=0°$, while this is not the case in Fig. 12(b). In Fig. 6, we saw that $\varphi(0)\neq 90°$ at $\phi=90°$ and in Appendix B we see that, for this behavior to occur, $|\tilde{f}_a''(\varphi(0)=90°)| > K_2/L_z$ is necessary. In the present cases of surface with square patterns $|\tilde{f}_a''(\varphi(0)=0°)|$ must be larger than K_2/L_z for $\varphi(0)$ to become unequal to 0° at $\phi=0$. We find from Fig. 9 that $|\tilde{f}_a''(\varphi(0)=0°)|$ for a surface with square patterns is obviously smaller for $K_s/K_3=0.6$ than for $K_s/K_3=1$. By comparing Figs. 3 and 9 and carefully looking at the vertical axes, we also see that $|\tilde{f}_a''(\varphi(0)=0°)|$ for a surface with square patterns is smaller than $|\tilde{f}_a''(\varphi(0)=90°)|$ for one-dimensional grooves. Therefore it is likely that $|\tilde{f}_a''(\varphi(0)=0°)|$ for $K_s/K_3=0.6$ is not large enough to result in $\varphi(0)\neq 0°$ at $\phi=0°$. We again emphasize the excellent agreement between the results obtained by methods A and B found in Fig. 9, in spite of the relatively large difference in the behavior of $\varphi(0)$ that can be seen in Fig. 12.

Finally, we discuss here why in the case of $qA=3\pi/16 K_s/K_3=0.6$ gives a relatively better agreement with theory than $K_s/K_3=1$. A similar tendency was found in the case of one-dimensional grooves in our previous study [34], and we attributed it to a good agreement between theoretical and numerical results in the profile of the azimuthal angle of the director throughout the system (see Fig. 3 of Ref. [34]).

Now we carry out a similar analysis for the present results in the case of a surface with square patterns for $qA=3\pi/16$.

In Fig. 13, the azimuth of the director $\varphi_{\boldsymbol{n}}\equiv\arctan(n_y/n_x)$ for $qA=3\pi/16$ and $\phi=10°$ is plotted as a function of z/L_z at all the grid points in our numerical system for $K_s/K_3=0.6$ and 1. We also show, by solid lines, the range of $\varphi_{\boldsymbol{n}}$ expected by a naive theoretical argument: $\varphi_{\boldsymbol{n}}$ should be the superposition of a uniform twist $\{\varphi_{\text{twist}}(z)\equiv\varphi(0)+[\phi-\varphi(0)]z/L_z\}$ and azimuthal distortions induced by surface grooves. Therefore $\varphi_{\boldsymbol{n}}$ is expected to be in the range $[\varphi_{\text{twist}}(z)-\arcsin[n_y^{\max}(z,\varphi(0))],\varphi_{\text{twist}}(z)+\arcsin[n_y^{\max}(z,\varphi(0))]]$. Here $n_y^{\max}(z,\varphi(0))$ is the maximum azimuthal distortion expected theoretically, whose explicit form is given in Appendix C. We also note that $\varphi(0)$ is determined by method A.

The forms of the azimuthal-angle profiles are quite different despite the fact that the sole difference between Figs. 13(a) and 13(b) arises from the choice of the surface elastic constant K_s. Therefore Fig. 13 again demonstrates the significant role played by surface elasticity. Figure 13(b) indicates that the azimuthal angle profile $\{\varphi_{\boldsymbol{n}}\}$ almost falls onto the region expected by the above naive theoretical argument for $K_s/K_3=1$, while we find from Fig. 13(a) that the theoret-

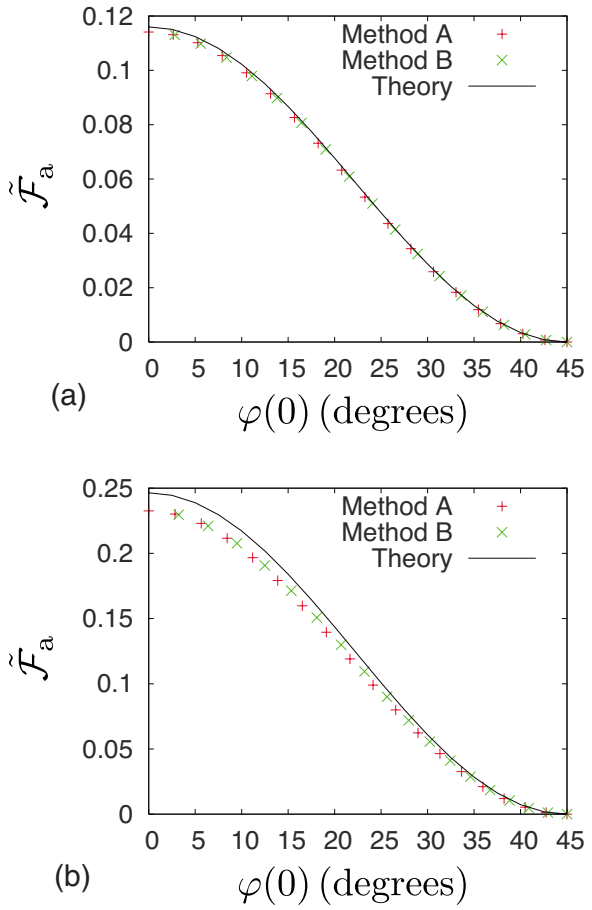

FIG. 8. (Color online) Same as Fig. 7 for $qA=\pi/16\simeq 0.196$.

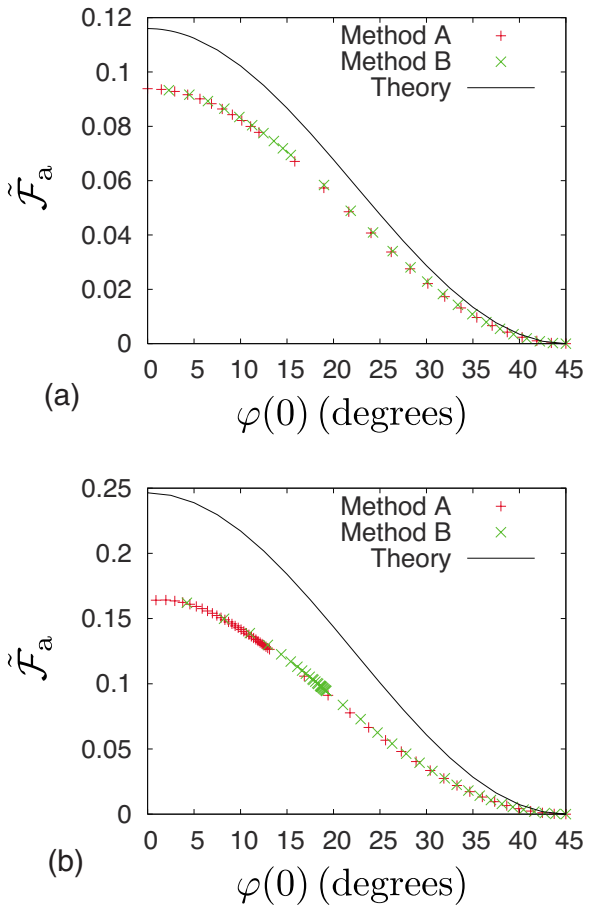

FIG. 9. (Color online) Same as Fig. 7 for $qA=3\pi/16\simeq 0.589$.

ical argument does not reproduce the calculated azimuthal angle profile, in particular close to $z=0$, for $K_s/K_3=0.6$. Considering the fact that $K_s/K_3=0.6$ gives a better agreement between theoretical and numerical anchoring energies, these results for the azimuthal angle profiles are somewhat surprising. The azimuthal angle profile for $K_s/K_3=0.6$ is almost symmetric about the line representing uniform twist [a line connecting $(z/L_z,\varphi_n)=(1,\phi)$ and $(0,\varphi(0))$, which is not drawn in Fig. 13]. On the other hand, it is highly asymmetric for $K_s/K_3=1$. Due to this symmetry of the azimuthal-angle profile, the contribution from the director deviating largely from the one naively expected from theoretical arguments might cancel out, which might be a reason for the better agreement between theoretical and numerical anchoring energies for $K_s/K_3=0.6$.

V. CONCLUSION

We carried out numerical calculations of anchoring energy of a grooved surface induced by the elastic distortions of a nematic liquid crystal in contact with the grooved surface. The present numerical study was motivated by our recent critical reexamination of Berreman's theory on surface anchoring of one-dimensional parallel grooves and its extension to surfaces with arbitrary shape. We checked whether our theoretical results for small surface slopes can be reproduced numerically, and what happens to surface anchoring energy when the surface slope cannot be regarded as small enough.

We studied the anchoring properties of a surface by imposing local planar degenerate anchoring (at which the director $\boldsymbol{n}$ can point to any direction as long as it is perpendicular to the local surface normal). We paid attention to surfaces whose height profile with respect to $z=0$ is written as $h(x,y)=A\sin qy$ (one-dimensional parallel grooves) or $h(x,y)=A(\sin qx+\sin qy)$ (surface with square patterns). We considered a nematic cell composed of the grooved surface and a flat surface imposing fixed $\boldsymbol{n}$ parallel to it. Since we dealt with a finite cell, twist deformations in the bulk exist and the total Frank elastic energy becomes the sum of the anchoring energy and the contribution from the uniform twist. Therefore to obtain information on the surface anchoring energy the twist contribution must be carefully eliminated. Moreover, to find out the azimuthal angle dependence of the anchoring energy, the "average" azimuthal angle at the grooved surface $\varphi(0)$ must be determined. To this end, we employed two methods; one is to determine $\varphi(0)$ by a simple extrapolation of the twist in the bulk, and the other relates $\varphi(0)$ to the derivative of the total Frank elastic energy with respect to ϕ.

We showed that both the methods give the same dependence of the anchoring energy on $\varphi(0)$, irrespective of the

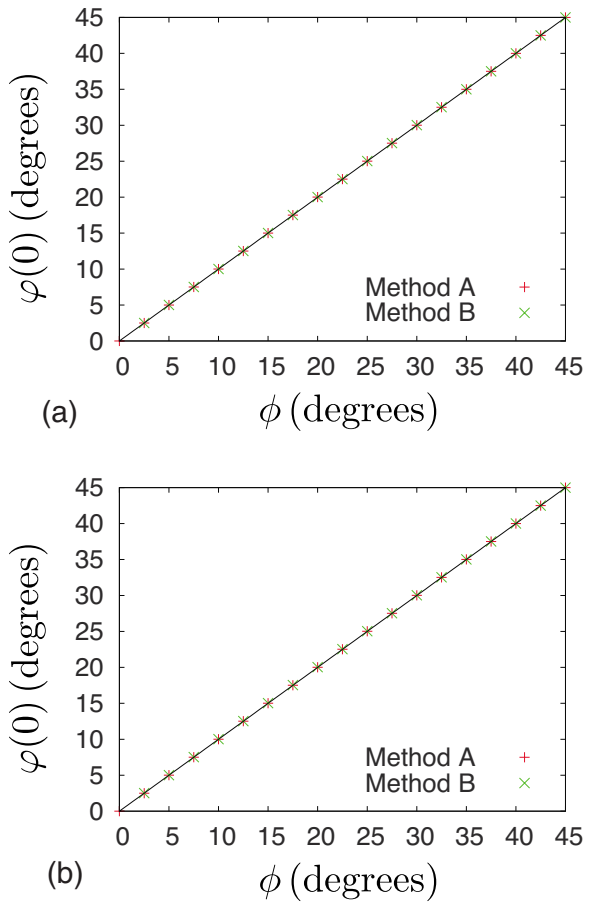

FIG. 10. (Color online) Azimuthal angle of the director at the bottom grooved surface with square patterns, $\varphi(0)$ as a function of the (fixed) azimuthal angle at the top flat surface ϕ for $qA=\pi/160\simeq 0.0196$. The surface elastic constant is $K_s/K_3=0.6$ (a) and 1 (b). The solid line corresponds to $\varphi(0)=\phi$, which implies the absence of twist deformations in the bulk.

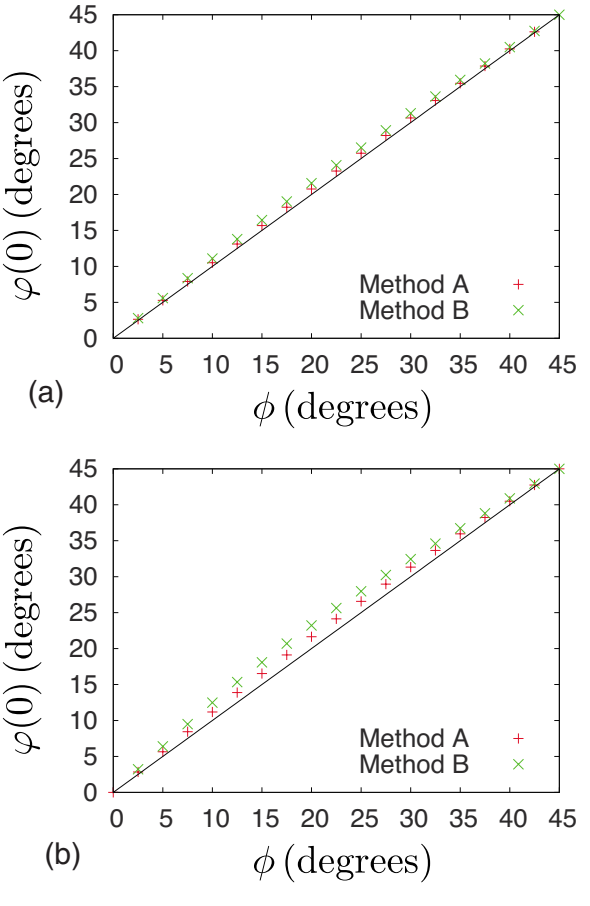

FIG. 11. (Color online) Same as Fig. 10 for $qA=\pi/16\simeq 0.196$.

shape of the surface (one-dimensional parallel grooves or a surface with square pattern), the surface slope qA, and the surface elastic constant K_s, although the variations of $\varphi(0)$ with respect to ϕ, (azimuth of the fixed director at the top surface) obtained by these two methods look slightly different. This result indicates that both methods are consistent and reliable as one for the determination of the azimuthal angle dependence of the anchoring energy of a grooved surface.

We found that for $qA\lesssim 0.2$ the agreement between analytical and numerical anchoring energies is excellent, for both one-dimensional parallel grooves and a surface with square patterns. Recalling the assumption of $|qA|\ll 1$ made in the theoretical argument, we can say that the applicability of the theory is larger than expected. We also observed a small twist deformation in the bulk when $qA\simeq 0.2$, while no observable twist is found for $qA\simeq 0.02$.

For a larger surface slope, $qA\simeq 0.59$, the results are quite different from those for $qA\lesssim 0.2$. As expected, deviation of the numerical anchoring energies from theory is clearly observed, although for one-dimensional grooves with $K_s/K_3=0.6$ the deviation is relatively small. Moreover, we observed the presence of large twist deformation in the bulk, and in the case of one-dimensional parallel grooves, perpendicular alignment $[\phi=\varphi(0)=90°]$ becomes unstable for $qA\simeq 0.6$, while it is stable for $qA\lesssim 0.2$. We demonstrated by a graphical argument that whether perpendicular alignment is stable or not is determined by the form of the anchoring energy and the value of K_2/L_z, with L_z being the cell thickness. In the case of a surface with square patterns, the deviation of numerical anchoring energies from analytical ones again depends on the surface elastic constant K_s. Nevertheless, the direction of the easy axis found from the numerical anchoring energy is along $\varphi(0)=45°$, in agreement with that of an analytical anchoring energy. We again found that $K_s/K_3=0.6$ gives a better agreement with theory than $K_s/K_3=1$. From these results, we can say that surface elasticity plays a crucial role in surface anchoring not only in the sense that the behavior of analytical anchoring energy sensitively depends on surface elastic constant as argued in our previous theoretical study, but also in the sense that the difference between numerical and analytical anchoring energy is dependent on surface elastic constant.

Before concluding this paper, we comment on several possible effects that have not been taken into account but might be important. For example, local reconstruction of the surface order with biaxiality could play some role in the case of strong surface distortions or in the presence of defects [43]. In treating such cases, description of the order should be done using a second-rank tensor Q_{ij} rather than a director $\boldsymbol{n}$. Furthermore, presmectic wetting might significantly influ-

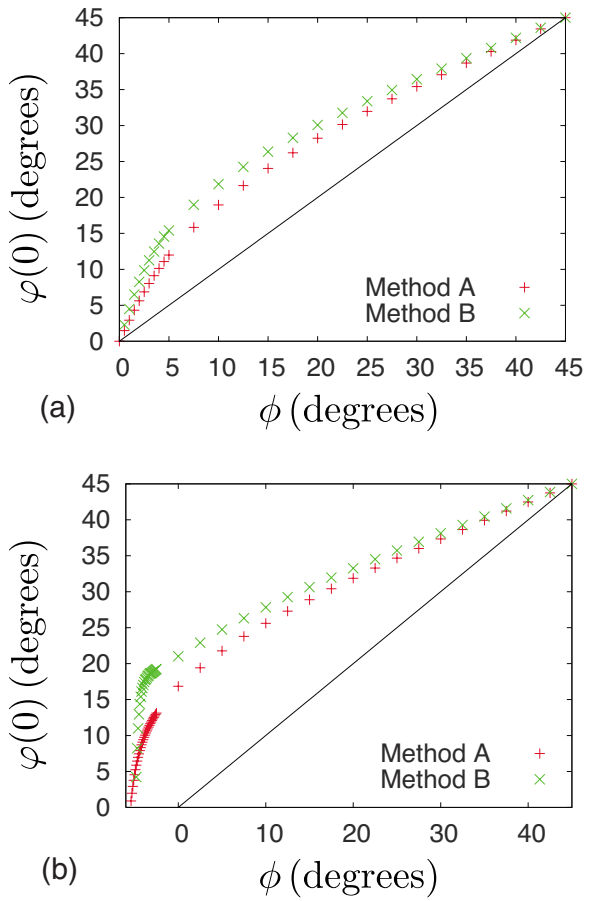

FIG. 12. (Color online) Same as Fig. 10 for $qA=3\pi/16 \simeq 0.589$.

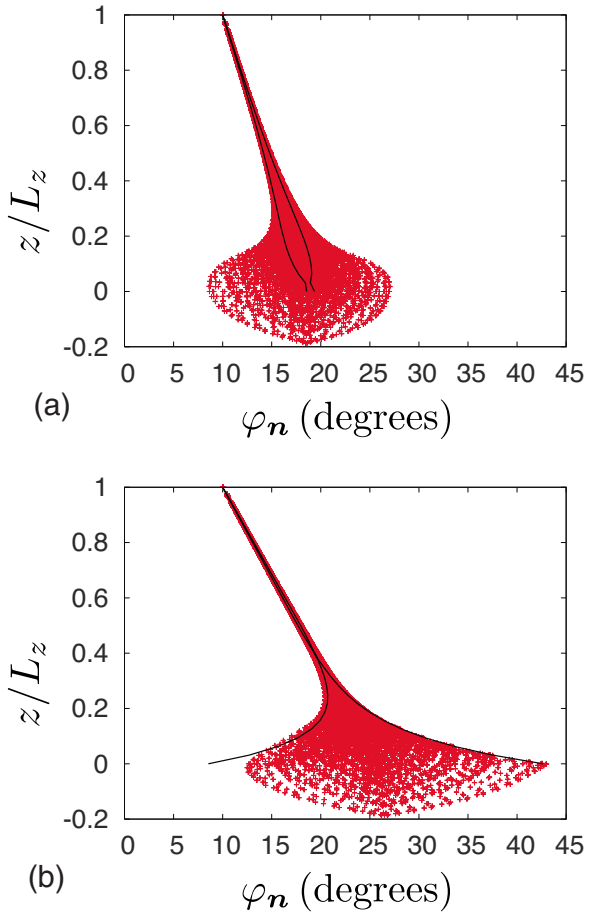

FIG. 13. (Color online) Distribution of the azimuth φ_n of the director with the variation of z/L_z in the case of $qA=3\pi/16$ and $\phi=10°$ for $K_s/K_3=$(a) 0.6 and (b) 1. Solid lines in each curve specify the region in which $\varphi_n(z)$ is expected to reside in a naive theoretical argument (see text).

ence surface phenomena, as has been shown experimentally in the case of porous materials in which geometry imposes strong frustration [44]. We also mention that a possibly important memory effect [45] has not been considered. Nevertheless, we believe that our numerical scheme will be a promising tool for the investigation of anchoring properties of grooved surfaces. Although here we restricted our analyses to one-dimensional sinusoidal grooves and a surface with square pattern whose height profile is given by a sum of two sinusoidal functions, our scheme can be readily extended to surfaces of general shape $h(x,y)$. Moreover, we can include local surface anchoring energy of the form, e.g., $W(\boldsymbol{n}\cdot\boldsymbol{\nu})$, in which W is an arbitrary function and $\boldsymbol{\nu}$ is some vector defined at each point of the surface, for example, the surface normal or a vector specifying the local easy direction. Considering the recent growing variety of experimental attempts to tailor microscopically patterned surfaces to control anchoring properties, we hope that the extension of our present work will help in understanding the anchoring properties of grooved surfaces manufactured experimentally, or in designing surfaces with desirable anchoring properties.

ACKNOWLEDGMENTS

This work is in part supported by KAKENHI (Grant-in-Aid for Scientific Research) on Priority Area "Soft Matter Physics" from the Ministry of Education, Culture, Sports, Science and Technology of Japan, and the Sasakawa Scientific Research Grant from the Japan Science Society.

APPENDIX A: DISCRETIZATION OF THE SYSTEM

In this appendix we will describe how to discretize the total Frank elastic energy F [Eq. (7)] and its functional derivatives $\delta F/\delta \boldsymbol{n}$. As noted in Sec. III A, we discretize the system by $N\times N\times(N+1)$ grid points with equal spacing $\Delta x=\Delta y=2\pi/qN$ in the x and y directions and $\Delta\zeta=L_z/N$ in the ζ direction. Equation (7) is formally discretized as

$$F=\frac{\Delta\zeta}{N^2}\sum_{i=0}^{N-1}\sum_{j=0}^{N-1}\sum_{k=0}^{N-1}\frac{\partial z}{\partial\zeta}f_{\mathrm{Frank}}^{\mathrm{cell}}(i,j,k), \tag{A1}$$

where $f_{\mathrm{Frank}}^{\mathrm{cell}}(i,j,k)$ is the Frank elastic energy density in a cell (i,j,k) whose volume is specified by $i\Delta x\leqslant x\leqslant(i+1)\Delta x$, $j\Delta\leqslant y\leqslant(j+1)\Delta y$, and $k\Delta\zeta\leqslant\zeta\leqslant(k+1)\Delta\zeta$. A derivative $\partial z/\partial\zeta$ appears explicitly in Eq. (A1) and f_{Frank} implicitly includes the derivatives $\partial z/\partial\zeta$, $\partial z/\partial x$, and $\partial z/\partial y$. Note that from Eq. (6) now z should be regarded as a function of x, y, and ζ. Since the functional form of $z(x,y,\zeta)$ is known from

Eq. (6), these derivatives can be readily calculated analytically. In the (i,j,k) cell, we evaluate those derivatives at the center of the cell, i.e., at $x=(i+1/2)\Delta x$, $y=(j+1/2)\Delta y$, and $\zeta=(k+1/2)\Delta\zeta$.

The Frank elastic energy density in a cell, $f_{\mathrm{Frank}}^{\mathrm{cell}}$, is a function of $\boldsymbol{n}$, $\partial_x\boldsymbol{n}$, $\partial_y\boldsymbol{n}$, and $\partial_\zeta\boldsymbol{n}$. For the following explanation, we define

$$\bar{\boldsymbol{n}}_{i,j,k}=\frac{1}{8}\sum_{i'=0}^{1}\sum_{j'=0}^{1}\sum_{k'=0}^{1}\boldsymbol{n}_{i+i',j+j',k+k'}, \tag{A2}$$

$$\bar{\partial}_x\boldsymbol{n}_{i,j,k}=\frac{\boldsymbol{n}_{i+1,j,k}-\boldsymbol{n}_{i,j,k}}{\Delta x},$$

$$\bar{\partial}_y\boldsymbol{n}_{i,j,k}=\frac{\boldsymbol{n}_{i,j+1,k}-\boldsymbol{n}_{i,j,k}}{\Delta y},$$

$$\bar{\partial}_\zeta\boldsymbol{n}_{i,j,k}=\frac{\boldsymbol{n}_{i,j,k+1}-\boldsymbol{n}_{i,j,k}}{\Delta\zeta}. \tag{A3}$$

Recall that the original Frank elastic energy density f_{Frank} is a function of $\boldsymbol{n}$, $\partial_x\boldsymbol{n}$, $\partial_y\boldsymbol{n}$, and $\partial_\zeta\boldsymbol{n}$, as is apparent in Eq. (7). With Eqs. (A2) and (A3) in mind, we define the discretized version of the Frank elastic energy density $f_{\mathrm{Frank}}^{\mathrm{cell}}(i,j,k)$ as

$$f_{\mathrm{Frank}}^{\mathrm{cell}}(i,j,k)=\frac{1}{8}\sum_{i'=0}^{1}\sum_{j'=0}^{1}\sum_{k'=0}^{1}f_{\mathrm{Frank}}(\bar{n}_{i,j,k},\bar{\partial}_x\boldsymbol{n}_{i,j+j',k+k'},\bar{\partial}_y\boldsymbol{n}_{i+i',j,k+k'},\bar{\partial}_\zeta\boldsymbol{n}_{i+i',j+j',k}). \tag{A4}$$

Once the equilibrium profile of $\{\boldsymbol{n}_{i,j,k}\}$ is known, the total Frank elastic energy can be calculated from Eqs. (A1) and (A4).

One might wonder why such a complicated form of a discretized Frank elastic energy density as Eq. (A4) is necessary, and think that a representative evaluation of a partial derivative in the cell like $\bar{\partial}_x\boldsymbol{n}=(1/4)\Sigma_{j'=0}^{1}\Sigma_{k'=0}^{1}(\boldsymbol{n}_{i+1,j+j',k+k'}-\boldsymbol{n}_{i,j+j',k+k'})$ would be sufficient. However, we found that such a treatment suffers from the checkerboard instability. A summation like $\Sigma_{j'=0}^{1}\Sigma_{k'=0}^{1}\boldsymbol{n}_{i,j+j',k+k'}$ smears out the checkerboardlike profile and thus cannot suppress the checkerboard instability once it occurs. This is the reason why we have chosen a complicated form of Eq. (A4), which can avoid the checkerboard instability.

To discuss how a functional derivative $\delta F/\delta\boldsymbol{n}$ should be defined, consider $G=\int_0^{2\pi/q}dx\int_0^{2\pi/q}dy\int_{h(x,y)}^{L_z}dz\,\psi(x,y,z)=\int_0^{2\pi/q}dx\int_0^{2\pi/q}dy\int_0^{L_z}d\zeta(\partial z/\partial\zeta)\psi(x,y,\zeta)$, where ψ is some scalar function. Evidently $\delta G/\delta\psi(x,y,z)=1$. On the other hand, after discretizing G in the same spirit, we have

$$\frac{\partial G}{\partial\psi_{i,j,k}}=\begin{cases}\dfrac{1}{2}\Delta x\Delta y\Delta\zeta\dfrac{\partial z}{\partial\zeta} & (k=0 \text{ or } N),\\ \Delta x\Delta y\Delta\zeta\dfrac{\partial z}{\partial\zeta} & (\text{otherwise}).\end{cases} \tag{A5}$$

Therefore the relation between a functional derivative and a discretized partial derivative is given by

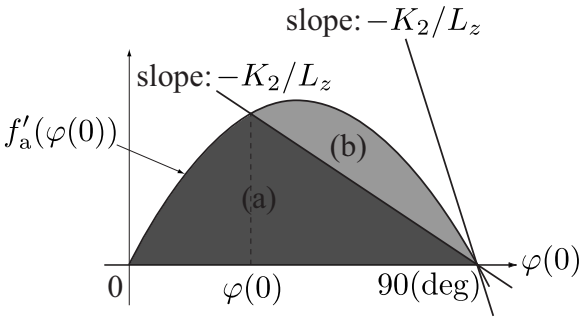

FIG. 14. Schematic illustration as to how to solve Eq. (9).

$$\frac{\delta G}{\delta\psi(x,y,z)}=\begin{cases}\dfrac{2}{\Delta x\Delta y\Delta\zeta\dfrac{\partial z}{\partial\zeta}}\dfrac{\partial G}{\partial\psi_{i,j,k}} & (k=0 \text{ or } N),\\ \dfrac{1}{\Delta x\Delta y\Delta\zeta\dfrac{\partial z}{\partial\zeta}}\dfrac{\partial G}{\partial\psi_{i,j,k}} & (\text{otherwise}).\end{cases} \tag{A6}$$

We use the same procedure to evaluate the functional derivative $\delta F/\delta\boldsymbol{n}(x,y,z)$ in the relaxation equation. Finally, we note that in Eqs. (A5) and (A6), $\partial z/\partial\zeta$ implies the average of the eight corresponding derivatives in the cells containing the vertex (i,j,k) ("eight" should be replaced by "four" when $k=0$ or N). But just for simplicity, in our numerical calculations, we evaluate $\partial z/\partial\zeta$ at $x=i\Delta x$, $y=j\Delta y$ and $\zeta=k\Delta\zeta$ in the calculation of Eq. (A6).

APPENDIX B: SCHEMATIC EXPLANATION OF SOME PROPERTIES OF $\varphi(0)$

In this appendix we first give a brief explanation as to why $\varphi(0)=90°$ at $\phi=90°$ (twist deformation is absent) when $qA=\pi/160\simeq0.0196$ and $\pi/16\simeq0.196$, while $\varphi(0)\neq90°$ (twist deformation is present) for $qA=3\pi/16\simeq0.589$. To this end, we illustrate schematically in Fig. 14 how to solve Eq. (9) when $\phi=90°$. In Fig. 14, the solution of Eq. (9) corresponds to the intersection of the curve representing $\tilde{f}_a'(\varphi(0))$ with a straight line with a slope $-K_2/L_z$. Notice from the symmetry of the system that $\tilde{f}_a'(\varphi(0)=0°)=\tilde{f}_a'(\varphi(0)=90°)=0$. For the cases we consider, $\tilde{f}_a'(\varphi(0))>0$ for $0°<\varphi(0)<90°$, as is evident from Figs. 1–3.

From Fig. 14, we readily find that when $|\tilde{f}_a''(\varphi(0)=90°)|\leq K_2/L_z$, with $f_a''(\varphi(0))=df_a'(\varphi(0))/d\varphi(0)$, Eq. (9) has no solution other than $\varphi(0)=90°$. The above condition implies weak surface anchoring or small cell thickness (or small L_z). On the other hand, when $|\tilde{f}_a''(\varphi(0)=90°)|>K_2/L_z$, there exists a solution $\varphi(0)<90°$, which corresponds to the presence of twist deformations in the bulk. We note that $\varphi(0)<90°$ always gives lower total free energy than that for $\varphi(0)=90°$, because from Eq. (8) the former equals the area of region (a) in Fig. 14, while the latter equals the sum of the areas of regions (a) and (b). Therefore, so long as a solution $\varphi(0)<90°$ exists, it always minimizes the total free energy;

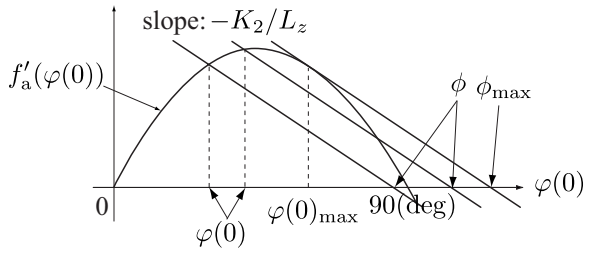

FIG. 15. Schematic illustration to explain why $\varphi(0) \leqslant \varphi(0)_{max} < 90°$.

in other words, the existence of a $\varphi(0) < 90°$ results in twist deformations in the bulk.

From Eq. (3), we have $\tilde{f}_a''(\varphi(0)=90°) = -KA^2q^3$, in which K is a function of K_1, K_2, K_3, and K_s and has the same dimension as that of those elastic constants [42]. From the discussion above, spontaneous twist deformations in the bulk exist when $KA^2q^3 > K_2/L_z$. Since we have chosen $L_z = 2\pi/q$ and $K_2 \simeq K$ as noted above, this condition leads to

$$2\pi(qA)^2 \gtrsim 1. \tag{B1}$$

Equation (B1) is satisfied when $qA = 3\pi/16 \simeq 0.6$, while it is not when $qA = \pi/16 \simeq 0.2$ or $qA = \pi/160 \simeq 0.02$. This argument is consistent with the presence of twist deformation in the bulk for $qA = 3\pi/16$ and its absence for $qA = \pi/16$ or $\pi/160$ in the case of $\phi = 90°$.

Next we show why $\varphi(0)$ cannot exceed some value $\varphi(0)_{max} < 90°$ in the case of $qA = 3\pi/16$ as found in Fig. 6. We again rely on a similar schematic illustration in Fig. 15, showing how $\varphi(0)$ is determined with the variation of ϕ. As in the above argument, $\varphi(0)$ is determined by the intersection of the curve representing $\tilde{f}_a'(\varphi(0))$ with a straight line with a slope $-K_2/L_z$. When ϕ is larger than some value ϕ_{max} indicated in Fig. 15, the line does not intersect with the curve $\tilde{f}_a'(\varphi(0))$, indicating that no solution exists, or that $\varphi(0)$ cannot be determined. When $\phi = \phi_{max}$, $\varphi(0)$ is evidently smaller than 90°. We note that this behavior is observed only when $|\tilde{f}_a''(\varphi(0)=90°)| > K_2/L_z$, which is the case for $qA = 3\pi/16$ as mentioned above. Otherwise, the line with a slope $-K_2/L_z$ always intersects the curve $\tilde{f}_a'(\varphi(0))$ and therefore $\varphi(0)$ can reach 90° when $\phi = 90°$.

APPENDIX C: EXPLICIT FORM OF $n_y^{max}(z, \varphi(0))$

In this appendix we will give the explicit form of the maximum azimuthal distortions $n_y^{max}(z, \varphi(0))$ necessary for plotting the solid lines in Fig. 13. We first briefly review our theoretical argument for one-dimensional parallel grooves [25,26]. Here we employ a setup equivalent to but apparently different from that in Sec. II. The director at infinity $\boldsymbol{n}_\infty$ is taken along the x direction and the height of the surface with respect to the reference plane $z=0$ reads $h(x,y) = A \sin[q(x \sin\phi + y \cos\phi)]$. Then the director $\boldsymbol{n}$ under the assumption of small distortion is written as $\boldsymbol{n} \simeq (1, n_y, n_z)$, in which n_y represents azimuthal distortions. The solution n_y for the present problem is given by $n_y(x,y,z,\phi) = qA \sin[q(x \sin\phi + y \cos\phi)]G(z,\phi)$, with [26]

$$G(z,\phi) = \sin\phi \left[\frac{\cos\phi}{g_1(\phi)} e^{-qzg_1(\phi)} + \frac{K_s}{K_3} \cot^2\phi \left(\frac{\cos\phi}{g_1(\phi)} e^{-qzg_1(\phi)} - \frac{g_2(\phi)}{\cos\phi} e^{-qzg_2(\phi)} \right) \right], \tag{C1}$$

in which the definition of $g_i(\phi)$ is found after Eq. (3) in Sec. II.

In the terminology of this appendix, the profile of the surface with square patterns is written as $h(x,y) = A(\sin q\tilde{x} + \sin q\tilde{y})$, where we have defined $\tilde{x} = x \sin\phi + y \cos\phi$ and $\tilde{y} = x \sin(\phi + \pi/2) + y \cos(\phi + \pi/2) = x \cos\phi - y \sin\phi$. We showed [27] that, as long as the distortion of the director is small enough, the superposition principle applies and therefore the azimuthal distortion n_y for the surface with square patterns reads $n_y(x,y,z,\phi) = qA[\sin(q\tilde{x})G(z,\phi) + \sin(q\tilde{y})G(z,\phi+\pi/2)]$. We notice that $\tilde{x}$ and $\tilde{y}$ can be varied independently. Therefore the maximum value of n_y with the variation of x and y (or $\tilde{x}$ and $\tilde{y}$) is given by

$$n_y^{max}(z,\phi) = qA[|G(z,\phi)| + |G(z,\phi+\pi/2)|]. \tag{C2}$$

We note here that, in the discussion of the main text, the angle ϕ is replaced by the azimuthal angle at the bottom, $\varphi(0)$, because the azimuthal angles of the director at the top and the bottom surfaces are generally different in our numerical system, and $\varphi(0)$ rather than ϕ is relevant to the behavior of the director in the vicinity of the bottom grooved surface (near the top flat surface, the director profile is just given by a uniform twist).

[1] P. G. de Gennes and J. Prost, *The Physics of Liquid Crystals*, 2nd ed. (Oxford University Press, Oxford, 1993).
[2] J. A. Castellano, Mol. Cryst. Liq. Cryst. **94**, 33 (1983).
[3] H. Yokoyama, in *Handbook of Liquid Crystal Research*, edited by P. J. Collings and J. S. Patel (Oxford University Press, Oxford, 1997), Chap. 6.
[4] J. Cheng and G. D. Boyd, Appl. Phys. Lett. **35**, 444 (1979).
[5] J. M. Geary, J. W. Goodby, A. R. Kmetz, and J. S. Patel, J. Appl. Phys. **62**, 4100 (1987).
[6] S. Ishihara, H. Wakemoto, K. Nakazima, and Y. Matsuo, Liq. Cryst. **4**, 669 (1989).
[7] M. Rüetschi, P. Grütter, J. Fünfschilling, and H.-J. Güntherodt, Science **265**, 512 (1994).
[8] B. Wen, M. P. Mahajan, and C. Rosenblatt, Appl. Phys. Lett. **76**, 1240 (2000); B. Wen and C. Rosenblatt, J. Appl. Phys. **89**, 4747 (2001).
[9] J.-H. Kim, M. Yoneya, J. Yamamoto, and H. Yokoyama, Appl. Phys. Lett. **78**, 3055 (2001); J.-H. Kim, M. Yoneya, and H. Yokoyama, Nature (London) **420**, 159 (2002).
[10] B. Zhang, F. K. Lee, O. K. C. Tsui, and P. Sheng, Phys. Rev.

Lett. **91**, 215501 (2003).
[11] F. K. Lee, B. Zhang, P. Sheng, H. S. Kwok, and O. K. C. Tsui, Appl. Phys. Lett. **85**, 5556 (2004).
[12] M. Honma, K. Yamamoto, and T. Nose, J. Appl. Phys. **96**, 5415 (2004).
[13] S. Varghese, G. P. Crawford, C. W. M. Bastiaansen, D. K. G. de Boer, and D. J. Broer, Appl. Phys. Lett. **86**, 181914 (2005).
[14] J. S. Gwag, M. Yoneya, and H. Yokoyama, in Proceedings of IDW '06, Otsu, Japan, 2006 (unpublished), p. LCT7-4L; J. S. Gwag, J. Fukuda, M. Yoneya, and H. Yokoyama, Appl. Phys. Lett. **91**, 073504 (2007); J. S. Gwag, M. Oh-e, M. Yoneya, H. Yokoyama, H. Satou, and S. Itami, J. Appl. Phys. **102**, 063501 (2007); J. S. Gwag, J. H. Kim, M. Yoneya, and H. Yokoyama, Appl. Phys. Lett. **92**, 153110 (2008).
[15] F. S. Yeung and H. S. Kwok, Appl. Phys. Lett. **88**, 063505 (2006); F. S. Yeung, J. Y. Ho, Y. W. Li, F. C. Xie, O. K. Tsui, P. Sheng, and H. S. Kwok, *ibid.* **88**, 051910 (2006).
[16] D. W. Berreman, Phys. Rev. Lett. **28**, 1683 (1972); , Mol. Cryst. Liq. Cryst. **23**, 215 (1973).
[17] S. Faetti, Phys. Rev. A **36**, 408 (1987).
[18] G. P. Bryan-Brown, M. J. Towler, M. S. Bancroft, and D. G. McDonnell, in *Proceedings of International Display Research Conference* (Society for Information Display, San Jose, 1994), p. 209.
[19] J.-B. Fournier and P. Galatola, Phys. Rev. E **60**, 2404 (1999).
[20] J. Elgeti and F. Schmid, Eur. Phys. J. E **18**, 407 (2005).
[21] L. Harnau, S. Kondrat, and A. Poniewierski, Phys. Rev. E **72**, 011701 (2005); **76**, 051701 (2007).
[22] E. S. Lee, P. Better, T. Miyashita, T. Uchida, M. Kano, M. Abe, and K. Sugawara, Jpn. J. Appl. Phys., Part 2 **32**, L1436 (1993).
[23] C. J. Newsome, M. O'Neill, R. J. Farley, and G. P. Bryan-Brown, Appl. Phys. Lett. **72**, 2078 (1998).
[24] R. Barberi, I. Dozov, M. Giocondo, M. Iovane, Ph. Martinot-Lagarde, D. Stoenescu, S. Tonchev, and L. V. Tsonev, Eur. Phys. J. B **6**, 83 (1998).
[25] J. Fukuda, M. Yoneya, and H. Yokoyama, Phys. Rev. Lett. **98**, 187803 (2007).
[26] J. Fukuda, M. Yoneya, and H. Yokoyama, Phys. Rev. Lett. **99**, 139902(E) (2007).
[27] J. Fukuda, J. S. Gwag, M. Yoneya, and H. Yokoyama, Phys. Rev. E **77**, 011702 (2008).
[28] P. Patrício, M. M. Telo da Gama, and S. Dietrich, Phys. Rev. Lett. **88**, 245502 (2002).
[29] L. A. Parry-Jones and S. J. Elston, J. Appl. Phys. **97**, 093515 (2005).
[30] T. J. Spencer and C. M. Care, Phys. Rev. E **74**, 061708 (2006).
[31] L. Harnau and S. Dietrich, Europhys. Lett. **73**, 28 (2006).
[32] G. Barbero, A. S. Gliozzi, M. Scalerandi, and L. R. Evangelista, Phys. Rev. E **77**, 051703 (2008).
[33] K. Kiyohara, K. Asaka, H. Monobe, N. Terasawa, and Y. Shimizu, J. Chem. Phys. **124**, 034706 (2006).
[34] J. Fukuda, M. Yoneya, and H. Yokoyama, Phys. Rev. E **77**, 030701(R) (2008).
[35] S. Chandrasekhar, *Liquid Crystals*, 2nd ed. (Cambridge University Press, Cambridge, U.K., 1992).
[36] E. G. Virga, *Variational Theories for Liquid Crystals* (Chapman and Hall, London, 1994).
[37] J. Nehring and A. Saupe, J. Chem. Phys. **54**, 337 (1971).
[38] C. Oldano and G. Barbero, Phys. Lett. **110A**, 213 (1985); , J. Phys. (Paris) **46**, 451 (1985).
[39] H. Yokoyama, Phys. Rev. E **55**, 2938 (1997).
[40] To be precise, in the functional derivative $\delta F/\delta \boldsymbol{n}$, F implies the total free energy of the system, not the free energy per unit surface area.
[41] J. L. Ericksen, Phys. Fluids **9**, 1205 (1966).
[42] In the case of small qA, the exact form of K can be calculated directly from Eq. (3). For large qA, estimation of K can be carried out from the numerical result for the anchoring energy as shown in, e.g., Fig. 3. However, from Fig. 3, we find that the deviation of the numerically calculated anchoring energy from the analytical one is not large, and therefore the estimated K does not significantly differ from the analytically calculated one.
[43] M. Ambrožič, S. Kralj, and E. G. Virga, Phys. Rev. E **75**, 031708 (2007).
[44] S. Kralj, G. Cordoyiannis, A. Zidanšek, G. Lahajnar, H. Amenitsch, S. Žumer, and Z. Kutnjak, J. Chem. Phys. **127**, 154905 (2007).
[45] M. I. Boamfa, S. V. Lazarenko, E. C. M. Vermolen, A. Kirilyuk, and T. Rasing, Adv. Mater. (Weinheim, Ger.) **17**, 610 (2005).